

Development of a PEM fuel cell equivalent circuit model with PINN-based parameter identification

Ismail Ait Taleb¹, Zakaria Kourab¹, Souad Tayane², Mohamed Ennaji¹, Jaafar Gaber³

¹Laboratory Complex Cyber Physical Systems (CCPS), National High School of Arts and Crafts, Hassan II University, Casablanca, Morocco

²Process Engineering and Environmental Laboratory, Faculty of Science and Technology Mohammedia, Hassan II University, Casablanca, Morocco

³Institute FEMTO-ST, CNRS, UTBM, Marie and Louis Pasteur University, Belfort, France

Article Info

Article history:

Received May 6, 2025

Revised Oct 6, 2025

Accepted Oct 17, 2025

Keywords:

Data driven parameter identification

Equivalent circuit model

Physics informed neural network

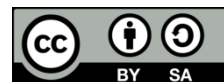
Proton exchange membrane fuel cell

Transient dynamic behavior prediction

ABSTRACT

This paper presents a novel equivalent electrical circuit model for proton exchange membrane fuel cells (PEMFCs) and introduces a physics-informed neural network (PINN) algorithm for parameter identification. The proposed model provides a more accurate representation of the fuel cell's dynamic behavior while maintaining computational efficiency. Unlike conventional methods, the PINN framework integrates physical constraints with data-driven learning, ensuring physically consistent parameter estimation. To validate its effectiveness, the proposed model is compared with the widely used RC equivalent circuit and a generic PEMFC model. Experimental data from a 1.2 kW PEMFC test bench serve as a benchmark for evaluating the transient and steady-state performance of each modeling approach. Results demonstrate that the proposed circuit, combined with PINN-based identification, yields enhanced accuracy in predicting voltage response under various operating conditions. Additionally, the model exhibits improved adaptability to transient phenomena compared to conventional equivalent circuits. These findings highlight the potential of physics-informed machine learning for advancing fuel cell modeling and control strategies.

This is an open access article under the [CC BY-SA](#) license.



Corresponding Author:

Ismail Ait Taleb

Laboratory Complex Cyber Physical Systems (CCPS), National High School of Arts and Crafts

Hassan II University

Casablanca, Morocco

Email: ismailaitaleb112@gmail.com

1. INTRODUCTION

The increasing global demand for sustainable energy solutions has driven significant interest in fuel cell technology as an alternative to conventional fossil-fuel-based energy sources. Among the various fuel cell types, the proton exchange membrane fuel cell (PEMFC) has emerged as a promising candidate, particularly for transportation, stationary power generation, and portable applications. PEMFCs offer numerous advantages, including high efficiency, low emissions, rapid startup, and the ability to operate at relatively low temperatures. In transportation, fuel cell electric vehicles (FCEVs) are gaining traction as a viable alternative to internal combustion engines and battery electric vehicles (BEVs), as they provide longer driving ranges, faster refueling times, and producing only water as a byproduct. However, the successful deployment of PEMFCs in real-world applications requires accurate modeling to predict their behavior under various operating conditions and develop effective control strategies [1]-[3].

Several modeling approaches have been developed to describe PEMFC behavior, ranging from electrochemical models based on fundamental reaction kinetics to dynamic state-space models and equivalent

circuit models [4]-[8]. Electrochemical models offer a detailed understanding of the physicochemical processes occurring within the fuel cell, but they rely on complex partial differential equations (PDEs) that require significant computational resources, making them impractical for real-time applications. To address these limitations, researchers have developed dynamic models, including state-space representations, which describe transient responses and operational dynamics more efficiently [9]-[13]. However, state-space models are highly nonlinear, requiring the identification of numerous parameters, which complicates their practical implementation.

Equivalent electrical circuit models provide a simplified yet effective representation of the electrical behavior of PEMFCs using standard components such as resistors, capacitors, and inductors. Among these, the RC equivalent circuit is widely used to model charge accumulation and transport processes due to its simplicity and computational efficiency. However, RC models often fail to accurately describe transient behavior, aging effects, and dynamic load variations. To improve representation, alternative frameworks such as the energetic macroscopic representation (EMR) have been developed, offering a graphical and structured method for analyzing energy interactions in PEMFCs. Despite their advantages, these models rely heavily on precise parameter estimation, which remains a significant challenge in equivalent circuit modeling.

One of the major difficulties in equivalent circuit models is accurately determining model parameters. Traditional parameter estimation techniques, such as electrochemical impedance spectroscopy (EIS) and least-squares optimization, require large amounts of experimental data and are highly sensitive to measurement noise and model assumptions [13]-[19]. To overcome these challenges, machine learning-based techniques have emerged as powerful tools for data-driven parameter estimation. In particular, physics-informed neural networks (PINNs) have gained increasing attention due to their ability to integrate physical constraints into neural network training, ensuring that estimated parameters remain physically meaningful while improving generalization across different operating conditions. This makes PINNs a promising approach for parameter estimation in fuel cell modeling [20]-[25].

In this study, a novel equivalent electrical circuit for PEMFCs is proposed, integrating a PINN-based algorithm for parameter identification. The new circuit is designed to enhance modeling accuracy by providing a more refined representation of both dynamic and steady-state behaviors, while ensuring computational efficiency. To evaluate its effectiveness, the proposed model is compared with existing approaches, including the RC equivalent circuit, the REM framework, and a generic PEMFC model. Experimental validation is performed using a 1.2 kW PEMFC test bench, allowing for a detailed assessment of the model's accuracy and adaptability across various operating conditions. By integrating physics-informed machine learning into equivalent circuit modeling, this research aims to bridge the gap between traditional analytical models and modern data-driven techniques, ultimately providing valuable insights for performance optimization, real-time control, and predictive diagnostics of PEMFC systems.

This paper is structured as follows: i) Section 2 outlines the theoretical principles of fuel cells, establishing the necessary background; ii) Section 3 presents the proposed equivalent electrical circuit model; iii) Section 4 details the PINN-based approach for parameter identification; iv) Section 5 describes the experimental setup and validation methodology; v) Section 6 analyzes the results, comparing the proposed model with existing ones and experimental findings; and vi) Finally section 7 summarizes the main conclusions and suggests potential directions for future research.

2. THEORETICAL PRINCIPLES OF FUEL CELL

Fuel cells generate electricity through electrochemical conversion, directly transforming chemical energy into electrical energy without combustion. In this regard, fuel cells share similarities with conventional batteries in their ability to produce electrical power. However, the fundamental distinction lies in the fact that fuel cells do not store energy internally; instead, they continuously generate electricity as long as fuel and oxidant are supplied. This makes fuel cells suitable for applications requiring sustained power generation, such as transportation, stationary power plants, and portable energy systems.

2.1. Structure and operating principle of a PEMFC

The structure of a hydrogen fuel cell comprises several key components, including a porous anode, a cathode, and a solid electrolyte membrane that separates the two electrodes, as shown in Figure 1. The anode serves as the site for fuel injection, where electrochemical oxidation of hydrogen occurs, while the cathode facilitates the reduction of oxygen, completing the redox reaction. This electrochemical process generates an electric current that flows through an external circuit, delivering power to a connected load. As part of the chemical reaction, hydrogen molecules entering the anode are dissociated into protons and electrons. The protons migrate through the electrolyte membrane, whereas the electrons travel through the external circuit, thereby generating usable electrical energy. At the cathode, the electrons recombine with protons and oxygen molecules to form water, which is expelled as a harmless byproduct [20].

Proton exchange membrane fuel cells (PEMFCs) utilize a solid polymer membrane as the electrolyte, which allows the selective passage of protons while blocking electron flow. The electrochemical reactions occurring at the electrodes are governed by (1) and (2).



The efficiency of PEMFCs depends on the operating temperature, pressure, and reactant concentration, which influence the overall voltage output. The highest voltage is observed under open-circuit conditions, but as current increases, the fuel cell experiences various voltage losses.

2.2. Fuel cell polarization curve and performance losses

The actual operating voltage of a fuel cell is lower than its theoretical maximum due to inherent losses that occur during operation. These losses define the characteristic polarization curve shown in Figure 2 and can be categorized into activation loss, ohmic loss, and concentration loss, each affecting performance at different current densities.

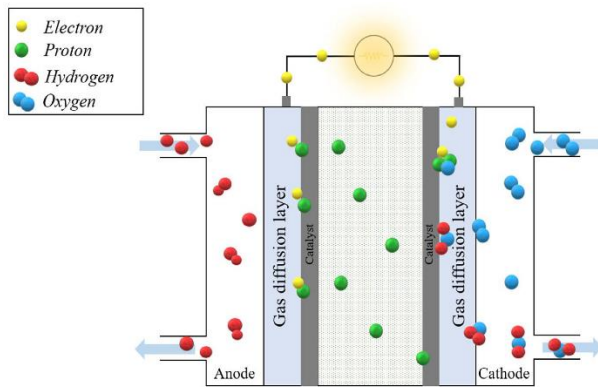


Figure 1. Fuel cell schematic

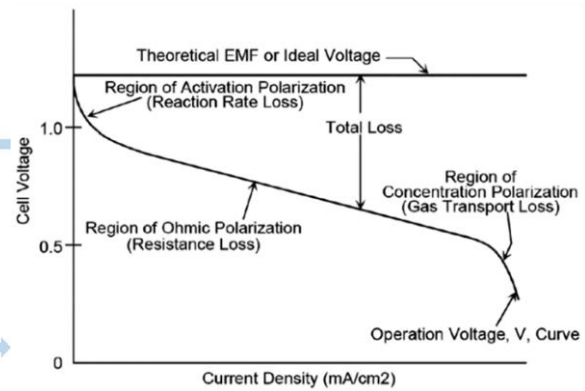


Figure 2. Polarization curve of a proton exchange membrane fuel cell (PEMFC)

2.2.1. Activation losses

These losses correspond to the voltage drop caused by the intrinsic sluggishness of electrochemical reactions at the electrodes. It is most pronounced at low current densities, where energy is required to overcome the activation barrier, particularly for the oxygen reduction reaction (ORR) at the cathode [5]. The use of high-efficiency catalysts, such as platinum, helps to reduce these losses. They are modeled using the Tafel equation as (3).

$$V_{act} = \frac{RT}{\alpha F} \ln \left(\frac{j}{j_0} \right) \quad (3)$$

j_0 is the exchange current density, which reflects the activity of the catalyst.

2.2.2. Ohmic losses

Ohmic losses are associated with resistive losses due to the electronic resistance in the electrodes and the ionic resistance in the electrolyte. Unlike activation losses, ohmic losses increase linearly with current density, leading to a steady voltage drop [5]. Using low-resistance materials and highly conductive membranes minimizes these losses. They are given by (4).

$$V_{ohmic} = iR_m \quad (4)$$

The membrane resistance (R_m) depends on membrane thickness, conductivity, and temperature, as (5).

$$R_m = \frac{t_m}{\sigma_m}, \quad \sigma_m = \sigma_m^0 \exp \left(-\frac{E_\sigma}{RT} \right) \quad (5)$$

2.2.3. Concentration losses

At high current densities, concentration losses occur due to mass transport limitations, where reactants become depleted at the electrode surface, reducing reaction rates and causing a sharp voltage drop. Proper gas diffusion layers (GDLs) and optimized flow channels help mitigate these effects, ensuring efficient reactant supply. Minimizing these losses is essential for improving fuel cell efficiency, durability, and overall system performance [5]. They are expressed as (6).

$$V_{concentration} = -\frac{RT}{F} \ln \left(1 - \frac{j}{j_{lim}} \right) \quad (6)$$

The limiting current density (j_{lim}) defines the maximum current the cell can support, based on reactant diffusion rates.

3. EQUIVALENT ELECTRICAL CIRCUIT

3.1. Proposed circuit

The proposed equivalent circuit model, shown in Figure 3, captures the transient electrochemical behavior of a PEMFC in the time domain by incorporating key resistive, capacitive, and inductive elements that describe its dynamic response. The ohmic resistance (R_{ohm}) accounts for ionic conduction losses within the electrolyte membrane and the electronic resistance of the electrodes and interconnects, directly influencing the instantaneous voltage drop. The activation resistance (R_{act}) characterizes the kinetic overpotential associated with the oxygen reduction reaction (ORR) at the cathode, which dominates at low current densities. The parallel branch consisting of R_0 and L defines the transient effects related to the adsorption/desorption of reaction intermediates, introducing an inductive response that affects the fuel cell's voltage recovery following variations in current demand. The charge transfer resistance (R_1) represents the direct faradaic processes that contribute to the overall reaction rate without being influenced by surface coverage dynamics. Additionally, the double-layer capacitance (C_{dl}) describes the charge accumulation at the electrode/electrolyte interface, which significantly impacts the voltage response to rapid current changes. This comprehensive approach yields a nuanced view of PEMFC behavior. It proves especially valuable under dynamic load conditions. In such contexts, transient phenomena play a decisive role. Such phenomena include charge redistribution, electrochemical reaction kinetics, and mass transport delays. Their inclusion enhances the fidelity of time-domain simulations. Consequently, the simulation framework serves as a robust analytical tool for design optimization. It facilitates the development of advanced control strategies. The primary aims are to mitigate transient losses, accelerate system response, and improve overall energy conversion efficiency.

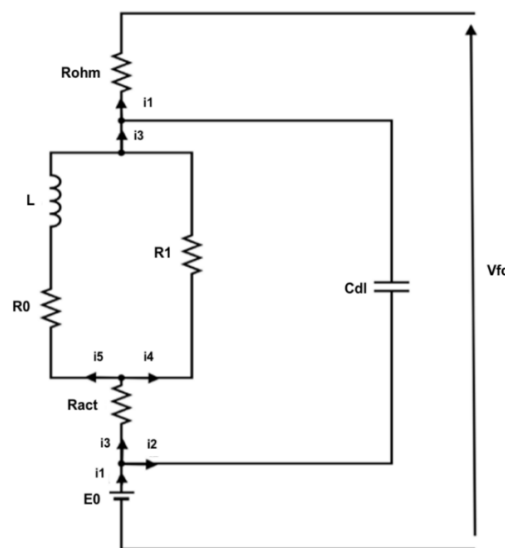


Figure 3. Proposed equivalent electrical circuit model for PEMFC

3.2. Determination of model parameters

Developing an equivalent circuit model for fuel cells demands the identification of core parameters. These include resistances, capacitances, and inductances that determine the system's dynamic response under different operating conditions. To accurately describe the fuel cell's electrical behavior, a set of governing

equations is established. These equations capture interactions among the circuit elements. They define voltage–current relationships and incorporate both steady-state and transient effects. Such formulations are essential for accurate parameter identification and enable effective system optimization. The governing equations of the proposed equivalent circuit model are expressed as (7)-(13).

$$V_{fc} = E - V_C - R_{ohm}i_1 \quad (7)$$

$$i_2 = C \cdot \frac{dV_C}{dt} \quad (8)$$

$$L \frac{di_5}{dt} + R_0 i_5 = R_1 i_4 \quad (9)$$

$$i_1 = i_2 + i_3 \quad (10)$$

$$i_3 = i_4 + i_5 \quad (11)$$

$$V_C = R_{act}i_3 + L \frac{di_5}{dt} + R_0 i_5 \quad (12)$$

$$V_{fc} = E - (R_{act} + R_{ohm})i_1 + R_{act}C \frac{dV_C}{dt} - L \frac{di_5}{dt} + R_0 i_5 \quad (13)$$

4. PHYSICS-INFORMED NEURAL NETWORKS (PINNS)

4.1. Introduction to PINNs

Physics-informed neural networks (PINNs) are a class of deep learning models that integrate physical laws into the training process. These laws are expressed as partial differential equations (PDEs) or ordinary differential equations (ODEs). Unlike traditional data-driven networks, PINNs leverage known physics to guide learning, reducing the need for large labeled datasets. It also improves model generalization. PINNs are particularly valuable in scientific computing. They can solve inverse problems, support system identification, and serve as surrogate models for complex physical systems [20]-[25].

4.2. PINN architecture and formulation

The formulation of a PINN involves integrating physics into the loss function, which constrains the network to satisfy both data-driven constraints and governing equations.

4.2.1. Neural network approximation

A PINN is structured as a deep neural network (DNN) parameterized by weights W and biases b , mapping an input x to an output \hat{f} , as (14).

$$\hat{f} = z^N = NN(x, W, b) \quad (14)$$

Where z^N represents the final layer of the neural network. The network is composed of multiple hidden layers with activation functions g , which introduce non-linearity into the model.

4.2.2. Physics-informed loss function

The fundamental aspect of PINNs is their physics-informed loss function, which consists of two major terms:

- Residual loss from governing equations: PINNs enforce the physics by incorporating differential equations into the training process. Given a differential operator \mathcal{L} , the network minimizes the residual error as (15).

$$L_f = \frac{1}{N_f} \sum_{i=1}^{N_f} \|\mathcal{L}[f(x)] - \phi(x)\|^2 \quad (15)$$

Where $\mathcal{L}[f(x)]$ is the governing differential equation applied to the predicted function $f(x)$, and $\phi(x)$ represents the known source term. N_f denotes the number of collocation points where the PDE residual is enforced.

- Boundary/initial condition loss: To ensure that the predicted function satisfies boundary or initial conditions, an additional term is introduced, as (16).

$$L_b = \frac{1}{N_b} \sum_{i=1}^{N_b} \|\mathfrak{B}[f(x)] - \psi(x)\|^2 \quad (16)$$

Where \mathfrak{B} represents the boundary condition operator, and $\psi(x)$ is the expected boundary/initial condition value.

- Data loss: In cases where observational or experimental data is available, an additional data loss term is introduced to align the model with known measurements, as (17).

$$L_d = \frac{1}{N_d} \sum_{i=1}^{N_d} \|f(x_i) - y_i\|^2 \quad (17)$$

Where N_d is the number of data points, y_i represents the observed values, and $f(x_i)$ is the network's prediction at those points. This term ensures that the model remains consistent with available empirical data.

4.2.3. Total loss function

The total loss function is defined as the sum of the individual contributions from the physics residuals, the data fidelity, and the boundary conditions. This formulation allows the PINN to incorporate both experimental information and physical constraints during training. By balancing these three components, the network achieves physical consistency while maintaining predictive accuracy, and it can be expressed as (18).

$$L = L_f + L_d + L_b \quad (18)$$

4.2.4. PINN training process

The training process of a PINN follows these steps: i) Initialize the neural network with random weights and biases; ii) Compute the output \hat{f} for given input x ; iii) Calculate derivatives of \hat{f} using automatic differentiation to enforce PDE constraints; iv) Compute the total loss function L by summing the residuals from the governing equations and boundary conditions; and v) Check for convergence:

- Check for convergence: If the loss function L falls below the predefined error tolerance ϵ , the training stops.
- Otherwise, parameters (W , b) are updated using an optimization algorithm, and the process repeats.

Figure 4 summarizes the steps described earlier and provides a schematic of a physics-informed neural network (PINN). The schematic illustrates how physical constraints integrate into the learning process. This iterative process ensures that the trained model learns a solution that satisfies both physical constraints and observed data.

4.3. Setting up the PINNs framework

Building on the earlier introduction of Physics-Informed Neural Networks (PINNs) and the governing equations of the proposed electrical equivalent circuit, this section presents a PINN-based parameter identification approach. The framework leverages a neural network to approximate key circuit variables. It enforces the ordinary differential equations governing the fuel cell's dynamic behavior. This design allows the simultaneous learning of state variables and circuit parameters. It achieves accurate results in a data-efficient manner.

4.3.1. Neural network approximation

A neural network $N_\theta(t)$ is defined with trainable parameters θ , where the network outputs two key quantities for each time t , as in (19).

$$[\hat{V}_c(t), \hat{i}_5(t)] = N_\theta(t) \quad (19)$$

Additionally, the physical parameters of the equivalent circuit model, such as: $\{E, R_{ohm}, R_{act}, R_0, R_1, L, C\}$ are treated as trainable parameters, denoted as θ_p . Thus, the overall trainable parameter set is as (20).

$$\theta = \theta_p \cup \theta_{nn} \quad (20)$$

Where θ_{nn} represents the neural network weights and biases, while θ_p includes the circuit parameters.

4.3.2. Physics-informed residuals (ODE constraints)

To enforce the governing physical equations, the derivatives of $\hat{V}_c(t)$ and $\hat{i}_5(t)$ with respect to time are computed using automatic differentiation. These derivatives are then substituted into the ODEs of the fuel cell equivalent circuit:

- Voltage residual

$$Res_1(t) = \widehat{V}_{fc}(t) - (E - \widehat{V}_c(t) - R_{ohm}i_1(t)) \quad (21)$$

- Capacitor current residual

$$Res_2(t) = i_2(t) - C \frac{d\widehat{V}_c(t)}{dt} = 0 \quad (22)$$

- Inductor current residual

$$Res_3(t) = L \frac{d\widehat{i}_5(t)}{dt} - R_0\widehat{i}_5(t) - R_{act}(i_1(t) - i_2(t)) = 0 \quad (23)$$

The residuals represent the differences between the left-hand and right-hand sides of the ODEs. These residuals are minimized during training to ensure that the predicted outputs satisfy the physical equations.

4.3.3. Data loss (measurement constraints)

The model incorporates experimental measurements of the fuel cell voltage and input current $\{V_{fc}(t_n), i_1(t_n)\}$. Typically, $i_1(t_n)$ is treated as an input (or boundary condition), while $V_{fc}(t_n)$ is used as a data constraint. The data loss function is defined as (24).

$$L_d = \frac{1}{N_d} \sum_{i=1}^{N_d} \|\widehat{V}_{fc}(t_n) - V_{fc,data}(t_n)\|^2 \quad (24)$$

This ensures that the predicted voltage $\widehat{V}_{fc}(t)$ aligns with the observed experimental data.

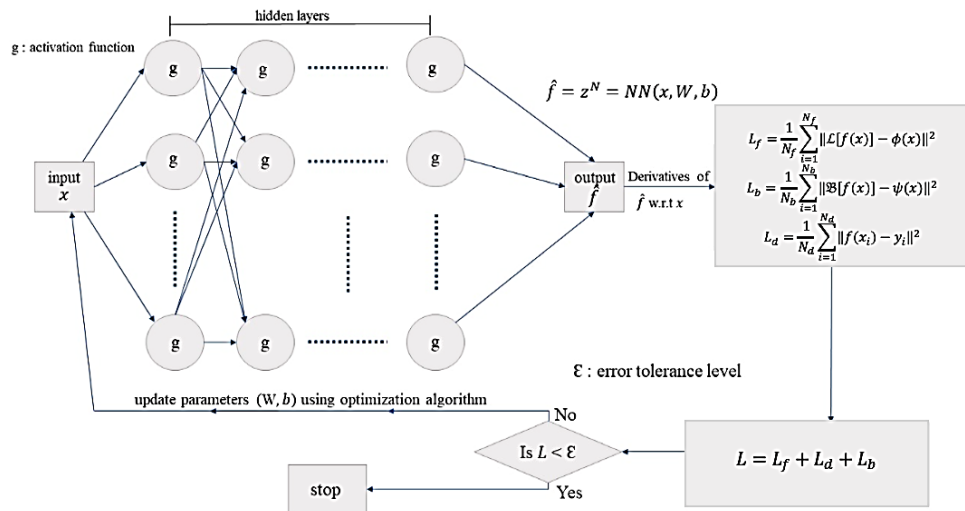


Figure 4. Schematic representation of PINN

4.3.4. Initial and boundary conditions

Initial conditions may be available for certain variables, such as $V_{fc}(t)$ and $i_5(t)$. If these values are known, they can be directly enforced. Otherwise, they can be treated as trainable parameters or approximated using initial guesses. A loss term is added to ensure consistency with initial conditions:

$$L_b = |\widehat{V}_c(0) - V_{c,0}|^2 + |\widehat{i}_5(0) - i_{5,0}|^2 \quad (25)$$

4.3.5. Total loss function

The overall loss function combines the physics residuals, data constraints, and initial condition enforcement:

$$L(\theta_p, \theta_{nn}) = \alpha_1 L_f + \alpha_2 L_d + \alpha_3 L_b \quad (26)$$

The parameters α_1 , α_2 , and α_3 in the total loss function, they serve as weighting coefficients that balance the contributions of different loss terms in the PINN framework.

5. MATERIALS AND METHODS

5.1. Experimental setup

To validate the developed model, experiments were conducted using the BAHIA didactic bench. This platform features 24 PEMFCs with a combined maximum power output of 1.2 kW and an output voltage range of 14 to 22 V, with a nominal current of 65 A. The BAHIA bench, as shown in Figure 5, is equipped with a human-machine interface (HMI), which allows for the precise configuration of the load current and enables the monitoring of the output voltage from the fuel cell. This setup facilitates a direct comparison between the experimental data and the results predicted by the proposed model.

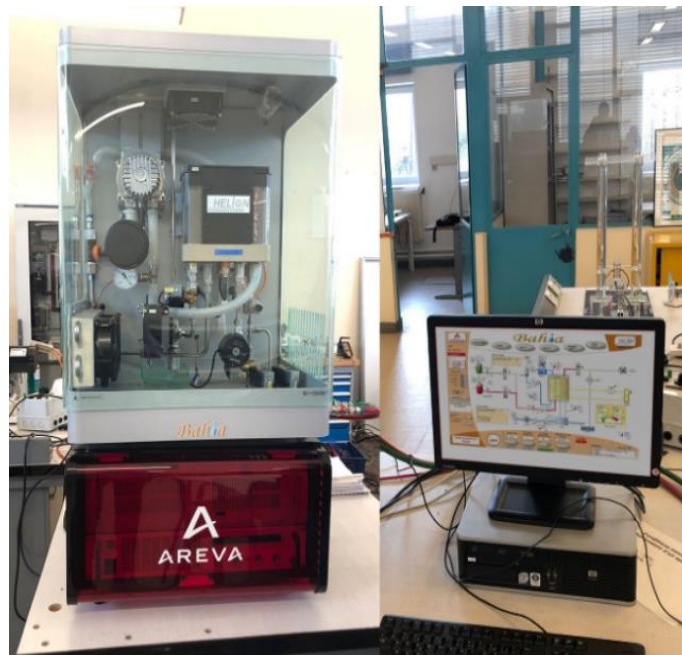


Figure 5. The PEMFC test bench

5.2. Simulation tools

To validate the proposed equivalent circuit model, simulations were performed using MATLAB/Simulink, while Python was used to run the PINNs for parameter identification, estimating the fuel cell's electrical and parameters.

5.2.1 MATLAB/Simulink for fuel cell modeling:

Two different MATLAB/Simulink-based models were utilized for comparison:

- Generic MATLAB PEMFC model: A Simscape-based generic PEM fuel cell (PEMFC) model was used to simulate fuel cell behavior under various operating conditions. This model provides a detailed, data-driven simulation, incorporating electrochemical and thermal dynamics. The specific configuration and parameter values are summarized in Table 1, while Figure 6 depicts the structure of this MATLAB model.
- Equivalent RC circuit model: A simplified resistor-capacitor (RC) equivalent circuit was employed for comparison, as illustrated in Figure 7. This model captures the electrical dynamics of the fuel cell. In particular, it represents charge transfer resistance and double-layer capacitance. This configuration enables a direct evaluation of transient responses. Consequently, the RC model provides a simplified yet insightful validation of dynamic effects [16].

Operating conditions were held constant across all simulations. The outputs from these models were compared systematically with experimental data. They were also evaluated against the proposed equivalent circuit model. This process provided a comprehensive validation approach.

Table 1. Parameters of the generic Simscape MATLAB/Simulink fuel cell model

Designation	Value	Designation	Value
Voltage at 0 A and 1 A	$V_0 = 22.65$ V $V_1 = 21$ V	Number of cells	$N = 24$
Nominal operating point	$V_{nom} = 15$ V $I_{nom} = 60$ A	Nominal supply pressure	$PO = 1$ bar $PH = 1.3$ bar
Maximum operating point	$I_{end} = 70$ A $V_{end} = 14.4$ V	Operating temperature	$T = 75$ °C

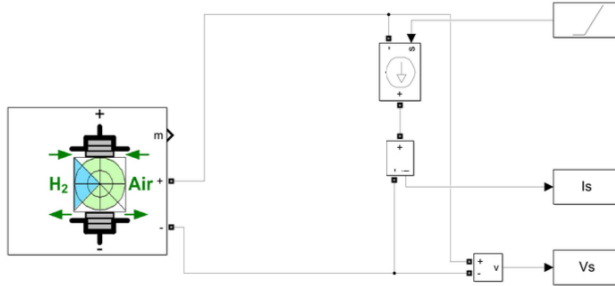


Figure 6. The generic MATLAB/Simulink Simscape model of a PEMFC

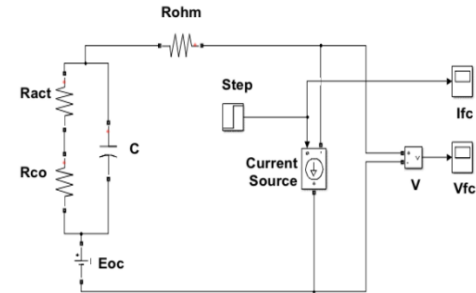


Figure 7. RC model

5.2.2. Python

In this study, Python was employed for parameter identification using physics-informed neural networks (PINNs). It estimated the fuel cell's electrical and electrochemical parameters. Python provides high computational efficiency. It also offers advanced optimization libraries. These features enabled accurate fitting of the equivalent circuit model to experimental data. This, in turn, ensured a reliable representation of the fuel cell's behavior.

5.2.3. Validation parameters

The accuracy of the proposed equivalent circuit model was assessed under static and dynamic conditions. These evaluations ensured its reliability for PEMFC performance analysis:

- Static testing: The model's predictions were compared with steady-state polarization curves to evaluate its ability to accurately estimate voltage across different current densities.
- Dynamic testing: Step changes in load current were applied. This tested the model's capacity to capture transient voltage responses. The analysis included the charge double-layer phenomenon and thermal dynamics.

The results from simulations and experimental measurements were used to validate the model's predictive capability and ensure its robustness under varying conditions.

6. RESULTS AND DISCUSSION

This section presents validation results for the proposed model. The model's outputs were compared with experimental test-bench data and with simulations from the generic MATLAB PEMFC model. A further comparison was made against the RC circuit model. The analysis evaluates both static and dynamic performance. These evaluations offer insights into the model's accuracy and its ability to predict fuel-cell behavior across various conditions.

6.1. Parameter identification using PINNs

The identification process aimed to represent the fuel cell's electrical behavior accurately. It relied on a dynamic state response driven by a pulse input current profile. The current varied between 20 A and 60 A, as shown in Figure 8. The PINN framework leveraged both experimental data and governing equations to estimate the circuit parameters. These parameters were used to refine the model, aligning it closely with real-world behavior. The identified parameters are presented in Table 2, capturing the key resistances, inductance, and capacitance influencing the fuel cell's electrical dynamics.

The distribution of prediction errors is shown in Figure 9, indicating that most errors are concentrated near zero, confirming the model's reliability in estimating fuel cell voltage responses. Additionally, the training loss, depicted in Figure 10, demonstrates a consistent reduction in total loss, data loss, and physics loss, validating the convergence of the PINN-based optimization.

Table 2. Root mean square error (RMSE) for PEMFC models compared to experimental data

Model	RMSE
MATLAB model	0.1561
Proposed model	0.2278
RC model	0.24139

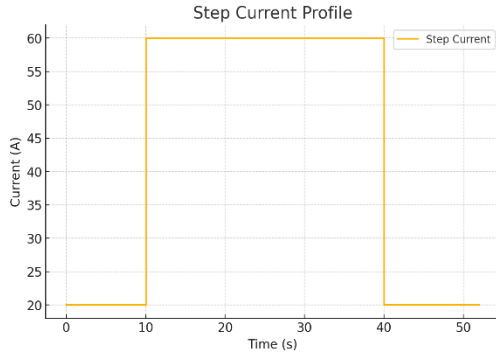


Figure 8. Input current profile

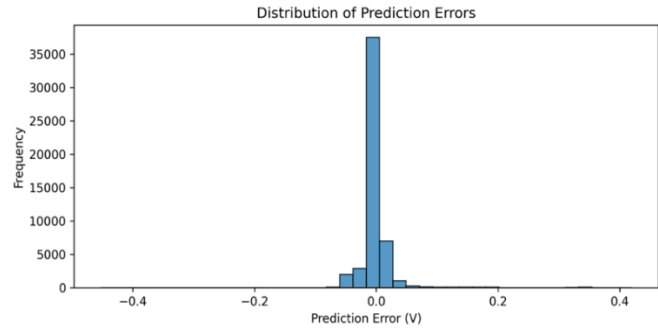


Figure 9. Distribution of prediction errors

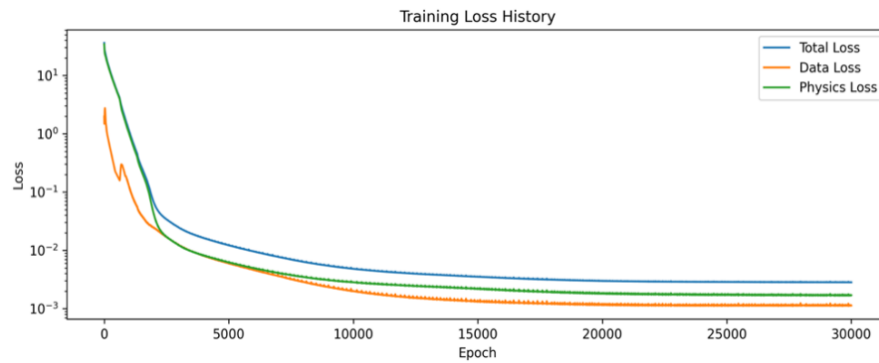


Figure 10. Training loss

6.2. Static performance analysis

The static behavior of the PEMFC was assessed by analyzing the voltage response under steady-state conditions, as shown in Figure 11. The comparison between the proposed model, the MATLAB generic model, and the RC model with experimental data from the test bench highlights the ability of these models to capture the fuel cell's behavior over time. The proposed model closely follows the experimental data, particularly during the initial phase of voltage decay, demonstrating its capability to represent the steady-state electrical characteristics of the PEMFC.

The voltage decay trend observed in all models reflects the dominant loss mechanisms within the fuel cell:

- Ohmic losses: The proposed model successfully captures the linear voltage drop in the steady-state region, showing accuracy comparable to the MATLAB generic model.
- Charge double-layer effect: The initial voltage relaxation phase is well represented by the RC model and the proposed equivalent circuit model, confirming their ability to capture electrical charge storage effects.
- Mass transport effects: The MATLAB model captures the concentration losses that become evident over time with high accuracy. The proposed model follows the same overall trend. However, it exhibits slight deviations during the later phase.

The root mean square error (RMSE) values in Table 2 provide a quantitative assessment of each model's accuracy. While the MATLAB PEMFC model demonstrates the highest precision with the lowest RMSE, the proposed model outperforms the RC model, highlighting its effectiveness in achieving a trade-off between computational efficiency and predictive accuracy, making it well-suited for practical applications.

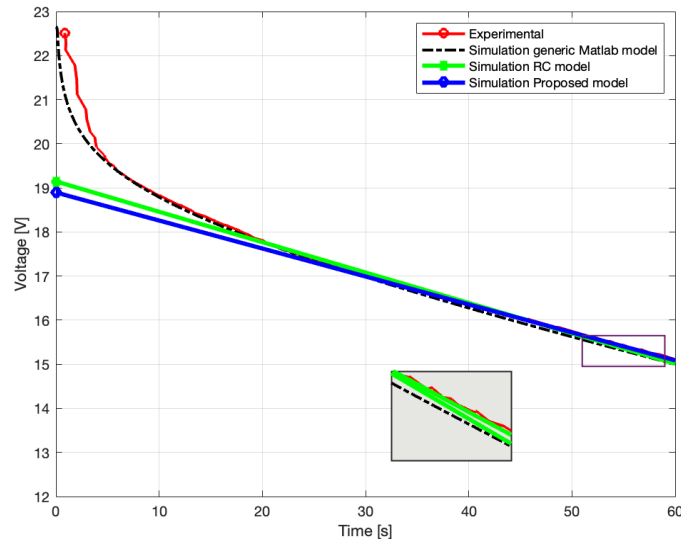


Figure 11. Comparison of static voltage response of PEMFC models with experimental data

6.3. Dynamic performance analysis

The transient voltage response of the proposed equivalent circuit model was evaluated under step changes in load current in comparison to other models, as shown in Figure 12. Using the identified parameters, the model effectively captures the initial voltage drop, charge redistribution effects, and recovery phase following the current variations. The ohmic resistance R_{ohm} , activation resistance R_{act} and capacitance C play a crucial role in shaping the voltage response. The presence of capacitance enables the proposed model to capture the charge double-layer effect, contributing to a more accurate representation of transient dynamics. The proposed model successfully follows the key transient features, particularly in voltage recovery after step changes.

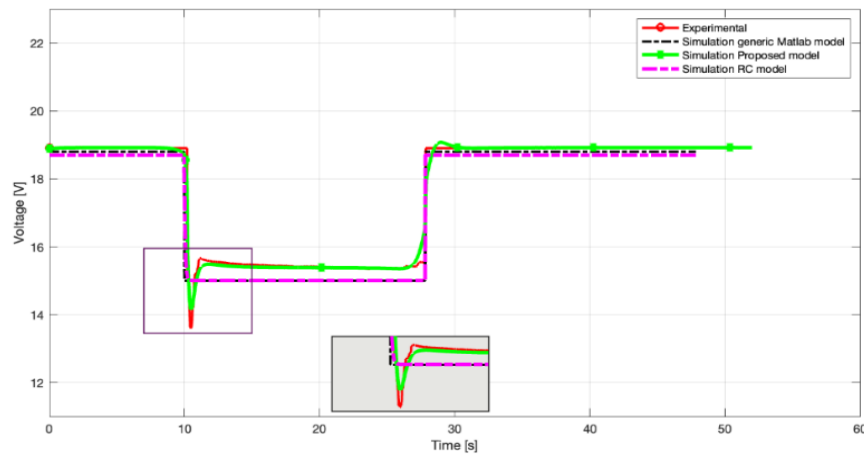


Figure 12. Comparison of the dynamic voltage response of PEMFC models with experimental data

Minor deviations appear in overshoot magnitude and the recovery phase, likely stemming from the inherent simplifications of the equivalent-circuit model. However, the proposed model maintains a balance between computational efficiency and predictive accuracy. This balance makes it suitable for real-time applications and integration into PEMFC control systems.

6.4. Sensitivity analysis

To assess the robustness of the proposed PINN-based equivalent circuit model, a local sensitivity analysis was conducted on three key parameters: ohmic resistance R_{ohm} , double-layer capacitance C , and inductance L . Each parameter was perturbed by both $\pm 10\%$ and $\pm 20\%$ relative to its identified optimum,

corresponding to multiplicative scaling factors of 0.8, 0.9, 1.1, and 1.2. After each perturbation, the PINN was briefly re-equilibrated and evaluated against the experimental dataset.

The results, illustrated in Figure 13, demonstrate that the model is most sensitive to variations in R_{ohm} . Deviations of $\pm 20\%$ caused a noticeable voltage offset and increased RMSE from ~ 0.106 V ($\pm 10\%$) to ~ 0.206 V ($\pm 20\%$), highlighting the critical influence of ohmic resistance on steady-state accuracy. By contrast, perturbations of C and L had only a marginal effect, with RMSE remaining close to 0.030–0.032 V, indicating that the model is comparatively robust to uncertainties in charge redistribution and inductive dynamics. Overall, the analysis confirms that the PINN framework retains stable predictive performance under moderate parameter deviations, while emphasizing that accurate identification of R_{ohm} is essential for reliable long-term operation modeling.

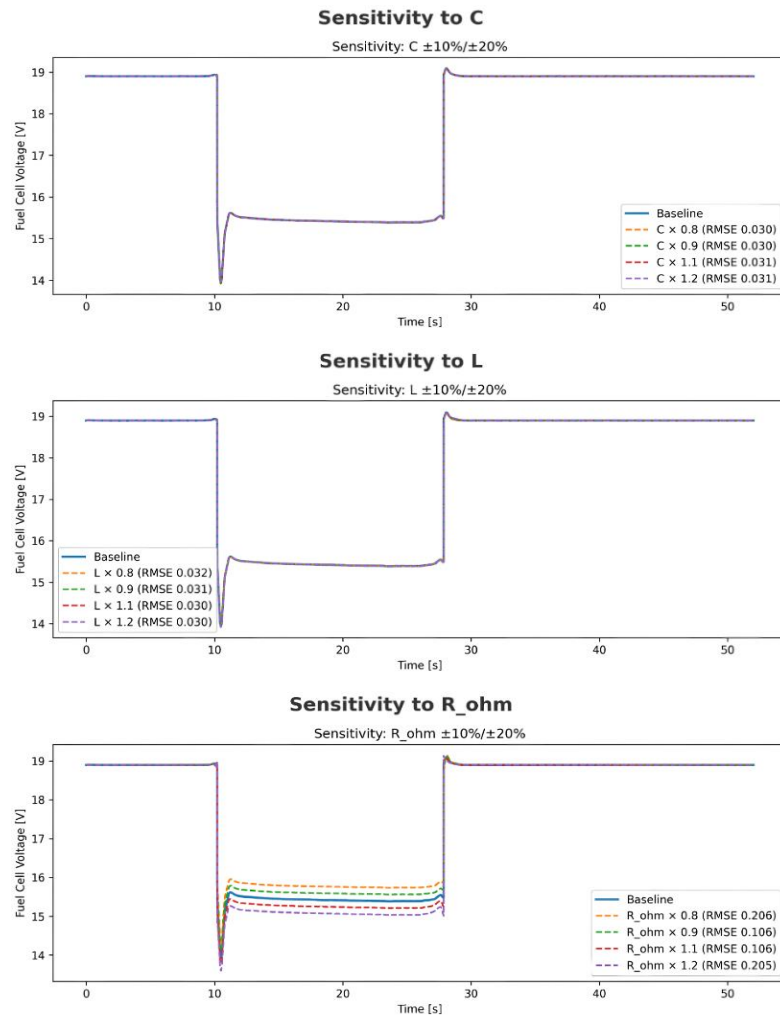


Figure 13. Sensitivity analysis of key PEMFC parameters under $\pm 10\%$ and $\pm 20\%$ perturbations: (a) C , (b) L , and (c) R_{ohm}

6.5. Comparative review of PEMFC modeling approaches

To further highlight the contribution of the proposed PINN-based equivalent-circuit model, a comparative analysis with recent PEMFC modeling approaches is presented in Table 3. Reinforcement learning methods such as PPO [16] achieve competitive accuracy but require GPU resources. Meta-heuristic optimizers, such as the hybrid aquila optimizer [12], also provide error reduction but are sensitive to convergence and computationally demanding. By contrast, the proposed PINN framework achieves the lowest RMSE while explicitly identifying physical parameters and maintaining practical convergence on both CPU and GPU platforms, making it well-suited for integration with power-electronic control applications.

Beyond benchmarking accuracy, the developed PINN-based equivalent-circuit model can be naturally embedded within power electronics systems. In practical applications, fuel cells are coupled with

DC-DC converters for maximum power point tracking and DC-link voltage regulation, and with inverters for motor drive control. By providing both accurate transient prediction and explicit equivalent-circuit parameters, the model can be integrated into converter control loops to improve load-following performance, reduce overshoot, and enable adaptive re-tuning under aging or fault conditions.

Table 3. Comparison of PINN with recent PEMFC approaches

Method	Dataset/bench	Metrics (RMSE)	Hardware used
Reinforcement learning (PPO) [16]	Nedstack PS6 6 kW	≈ 0.26 V;	GPU
Hybrid Aquila Optimizer (Meta-heuristic) [12]		≈ 0.28 V;	CPU
PINN + equivalent circuit	1.2 kW Bahia bench	0.2278 V;	CPU/GPU

7. CONCLUSION

This study developed and validated an electrical equivalent circuit model for a proton exchange membrane fuel cell (PEMFC). It introduced a physics-informed neural network (PINN) based approach for parameter identification. The proposed circuit model captures both steady state and transient electrical behavior. It maintains computational efficiency, making it suitable for real-time applications. The PINN integration ensures that estimated parameters align with experimental data. It also guarantees consistency with the physical principles governing PEMFC operation.

Validation involved comparisons with experimental test bench data and MATLAB-based simulations. The MATLAB models included both the generic PEMFC model and an RC circuit model. These comparisons demonstrated that the proposed model accurately reproduces fuel cell voltage dynamics. Under steady state conditions, it captured ohmic and charge storage effects and aligned well with experimental polarization curves. Under dynamic conditions, it predicted voltage transients in response to load variations. It also captured key phenomena such as initial voltage drops, charge redistribution, and recovery dynamics. The quantitative error analysis, particularly the RMSE values, confirms the effectiveness of the PINN-identified parameters in enhancing model accuracy, reducing deviations from experimental measurements, and improving predictive reliability.

The methodology presented establishes a computationally efficient and physically consistent framework for fuel cell modeling, bridging the gap between simplified circuit-based representations and high-fidelity physics-based simulations. Beyond standalone modeling, the framework can also be embedded within power electronic control loops—such as DC-DC converters for maximum power point tracking and DC-link voltage regulation, or inverters in electric drive systems—where its predictive capability enhances load-following behavior, improves transient response, and supports fault-tolerant operation. While detailed numerical models remain the most precise, the proposed approach offers a scalable and adaptable alternative for real-time applications, including fuel cell diagnostics, energy management, and control system design. Future work will focus on refining parameter estimation, integrating temperature effects, and modeling long-term degradation to enhance fuel cell performance prediction.

FUNDING INFORMATION

Authors state no funding involved.

AUTHOR CONTRIBUTIONS STATEMENT

This journal uses the Contributor Roles Taxonomy (CRediT) to recognize individual author contributions, reduce authorship disputes, and facilitate collaboration.

Name of Author	C	M	So	Va	Fo	I	R	D	O	E	Vi	Su	P	Fu
Ismail Ait Taleb	✓	✓	✓	✓	✓	✓	✓	✓	✓	✓			✓	
Zakaria Kourab	✓	✓				✓				✓	✓			
Souad Tayane	✓	✓		✓	✓		✓		✓		✓	✓	✓	
Mohamed Ennaji	✓	✓	✓	✓		✓		✓		✓		✓		
Jaafar Gaber	✓	✓	✓	✓	✓			✓	✓			✓		

C : Conceptualization	I : Investigation	Vi : Visualization
M : Methodology	R : Resources	Su : Supervision
So : Software	D : Data Curation	P : Project administration
Va : Validation	O : Writing - Original Draft	Fu : Funding acquisition
Fo : Formal analysis	E : Writing - Review & Editing	

CONFLICT OF INTEREST STATEMENT

Authors state no conflict of interest.

DATA AVAILABILITY




The data that support the findings of this study are available from the corresponding author, [IAT], upon reasonable request.

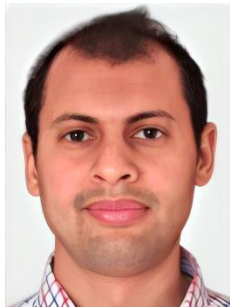
REFERENCES




- [1] E. Ogungbemi, T. Wilberforce, O. Ijaodola, J. Thompson, and A. G. Olabi, "Selection of proton exchange membrane fuel cell for transportation," *International Journal of Hydrogen Energy*, vol. 46, no. 59, pp. 30625–40, 2021, doi: 10.1016/j.ijhydene.2020.06.147.
- [2] R. Qi and L.-Z. Zhang, "Multi-scale modelling on PEM-based electrolyte dehumidifier: Transient heat and mass transfer in anode catalyst layer with microstructures," *International Journal of Heat and Mass Transfer*, vol. 179, p. 121720, Nov. 2021, doi: 10.1016/j.ijheatmasstransfer.2021.121720.
- [3] R. Kaiser, C.-Y. Ahn, Y.-H. Kim, and J.-C. Park, "Towards reliable prediction of performance for polymer electrolyte membrane fuel cells via machine learning-integrated hybrid numerical simulations," *Processes*, vol. 12, no. 6, p. 1140, 2024, doi: 10.3390/pr12061140.
- [4] M. Haidoury *et al.*, "Hybrid fuel cell-supercapacitor system: modeling and energy management using Proteus," *International Journal of Electrical and Computer Engineering (IJECE)*, vol. 14, no. 1, p. 110, Feb. 2024, doi: 10.11591/ijece.v14i1.pp110-128.
- [5] M. Haidoury, A. El Fatimi, H. Jbari, and M. Rachidi, "Modeling of fuel cell by using proteus," in *2022 IEEE 3rd International Conference on Electronics, Control, Optimization and Computer Science (ICECOCS)*, IEEE, 2022, pp. 1–5. doi: 10.1109/ICECOCS55148.2022.9983222.
- [6] S. E. Hosseini, "Fundamentals of hydrogen fuel cell systems," in *Fundamentals of Hydrogen Production and Utilization in Fuel Cell Systems*, Elsevier, 2023, pp. 255–282. doi: 10.1016/B978-0-323-88671-0.00007-3.
- [7] R. Gass, Z. Li, R. Outbib, S. Jemei, and D. Hissel, "A critical review of proton exchange membrane fuel cells matter transports and voltage polarisation for modelling," *Journal of The Electrochemical Society*, vol. 171, no. 3, p. 034511, Mar. 2024, doi: 10.1149/1945-7111/ad305a.
- [8] N. A. Dotzauer, "Dynamic modeling of fuel cells for applications in aviation," in *EASN 2024*, Basel Switzerland: MDPI, Mar. 2025, p. 68. doi: 10.3390/engproc2025090068.
- [9] K. Sun, I. Esnaola, O. Okorie, F. Chamley, M. Moreno, and A. Tiwari, "Data-driven modeling and monitoring of fuel cell performance," *International Journal of Hydrogen Energy*, vol. 46, no. 66, pp. 33206–33217, Sep. 2021, doi: 10.1016/j.ijhydene.2021.05.210.
- [10] L. Zhao, H. Dai, F. Pei, P. Ming, X. Wei, and J. Zhou, "A Comparative study of equivalent circuit models for electro-chemical impedance spectroscopy analysis of proton exchange membrane fuel cells," *Energies*, vol. 15, no. 1, p. 386, Jan. 2022, doi: 10.3390/en15010386.
- [11] D. H. Trinh, Y. Kim, and S. Yu, "One-dimensional dynamic model of a PEM fuel cell for analyzing through-plane species distribution and irreversible losses under various operating conditions," *Case Studies in Thermal Engineering*, vol. 60, p. 104815, Aug. 2024, doi: 10.1016/j.csite.2024.104815.
- [12] M. K. Singla *et al.*, "Revolutionizing proton exchange membrane fuel cell modeling through hybrid aquila optimizer and arithmetic algorithm optimization," *Scientific Reports*, vol. 15, no. 1, p. 5122, Feb. 2025, doi: 10.1038/s41598-025-89631-8.
- [13] P. R. Pathapati, X. Xue, and J. Tang, "A new dynamic model for predicting transient phenomena in a PEM fuel cell system," *Renewable Energy*, vol. 30, no. 1, pp. 1–22, Jan. 2005, doi: 10.1016/j.renene.2004.05.001.
- [14] M. Seddiq, M. Alnajideen, and R. Navaratne, "Thermal transient performance of PEM fuel cells in aerospace applications: a numerical study," *Energy & Fuels*, vol. 39, no. 16, pp. 7876–7889, Apr. 2025, doi: 10.1021/acs.energyfuels.4c04834.
- [15] G. K. K. M. and U. S., "An intelligent parametric modeling and identification of a 5 kW ballard PEM fuel cell system based on dynamic recurrent networks with delayed context units," *International Journal of Hydrogen Energy*, vol. 46, no. 29, pp. 15912–15927, Apr. 2021, doi: 10.1016/j.ijhydene.2021.02.065.
- [16] N. M. Salem, M. A. M. Shaheen, and H. M. Hasanien, "Novel reinforcement learning technique based parameter estimation for proton exchange membrane fuel cell model," *Scientific Reports*, vol. 14, no. 1, p. 27475, Nov. 2024, doi: 10.1038/s41598-024-78001-5.
- [17] R. Almodfer *et al.*, "Improving parameter estimation of fuel cell using honey badger optimization algorithm," *Frontiers in Energy Research*, vol. 10, no. May, pp. 1–12, 2022, doi: 10.3389/fenrg.2022.875332.
- [18] J. Wang, Q. Peng, J. Meng, T. Liu, J. Peng, and R. Teodorescu, "A physics-informed neural network approach to parameter estimation of lithium-ion battery electrochemical model," *Journal of Power Sources*, vol. 621, p. 235271, Nov. 2024, doi: 10.1016/j.jpowsour.2024.235271.
- [19] T. Ko, D. Kim, J. Park, and S. H. Lee, "Physics-informed neural network for long-term prognostics of proton exchange membrane fuel cells," *Applied Energy*, vol. 382, p. 125318, Mar. 2025, doi: 10.1016/j.apenergy.2025.125318.
- [20] E. Kharazmi, M. Cai, X. Zheng, Z. Zhang, G. Lin, and G. E. Karniadakis, "Identifiability and predictability of integer- and fractional-order epidemiological models using physics-informed neural networks," *Nature Computational Science*, vol. 1, no. 11, pp. 744–753, Nov. 2021, doi: 10.1038/s43588-021-00158-0.
- [21] A. Farea, O. Yli-Harja, and F. Emmert-Streib, "Understanding physics-informed neural networks: techniques, applications, trends, and challenges," *AI*, vol. 5, no. 3, pp. 1534–1557, Aug. 2024, doi: 10.3390/ai5030074.
- [22] G. E. Karniadakis, I. G. Kevrekidis, L. Lu, P. Perdikaris, S. Wang, and L. Yang, "Physics-informed machine learning," *Nature Reviews Physics*, vol. 3, no. 6, pp. 422–440, May 2021, doi: 10.1038/s42254-021-00314-5.
- [23] X. Jin, S. Cai, H. Li, and G. E. Karniadakis, "NSFnets (Navier-Stokes flow nets): Physics-informed neural networks for the incompressible Navier-Stokes equations," *Journal of Computational Physics*, vol. 426, 2021, doi: 10.1016/j.jcp.2020.109951.
- [24] A. Kovacs *et al.*, "Conditional physics informed neural networks," *Communications in Nonlinear Science and Numerical Simulation*, vol. 104, p. 106041, Jan. 2022, doi: 10.1016/j.cnsns.2021.106041.
- [25] M. Raissi, P. Perdikaris, and G. E. Karniadakis, "Physics informed deep learning," 2019. [Online]. Available: <https://maziarraissi.github.io/PINNs/>. Accessed: May 5, 2025.

BIOGRAPHIES OF AUTHORS






Ismail Ait Taleb    was born in Marrakesh, Morocco, in 1996. He received his engineering degree in Aeronautical Engineering in 2019. He is currently pursuing a Ph.D. at the National Higher School of Arts and Crafts (ENSAM Casablanca) in the Complex Cyber Physical Systems (CCPS) Laboratory in Casablanca, Morocco. His research interests include energy management systems, artificial intelligence applied to renewable energy, and the modeling and optimization of multi-source energy systems. He can be contacted at email: ismailaitaleb112@gmail.com.






Zakaria Kourab    was born in Casablanca, Morocco, in 1987. He received an engineer's degree in electromechanics from the National High School of Arts and Crafts (ENSAM-Meknes) in 2012. Currently, he is pursuing a Ph.D. with the National High School of Arts and Crafts (ENSAM-Casablanca), in the laboratory Complex Cyber Physical Systems (CCPS), Casablanca, Morocco. His research focuses on energy management systems, modeling, and control of multi-source systems. He can be contacted at email: zakaria.kourab@gmail.com.






Souad Tayane    is a professor of industrial chemistry at the Faculty of Science and Technology, Mohammedia, specializing in research on smart, bio-based, and biomaterials. She obtained her HDR in Industrial Chemistry at Hassan II University in Casablanca and was a researcher at Louis Pasteur University in Strasbourg. She is also an ILO-accredited trainer of trainers in entrepreneurship and project management. She has held editorial positions, chaired national and international workshops, and is Secretary General of the Moroccan Association of Green and Alternative Energies (AMEVA). She can be contacted at email: souadtayane2013@gmail.com.



Mohamed Ennaji    was born in Casablanca, Morocco, in 1983. He received the master's degree in industrial systems engineering, aeronautical option from the Évre Val-d'Essonne University, (Évre-Courcouronnes) in 2008. Also, he earned his Ph.D. in Electrical Engineering, specializing in Wind turbine modeling at ENSEM in 2015. He is also a professor of mechatronics, computer-aided design, and manufacturing. He is head of the Rapid Prototyping Laboratory at the National School of Arts and Crafts of Casablanca. He is involved in various research projects, on topics such as new actuator technologies, new rapid prototyping processes, programmable matter, exoskeletons, and Unmanned Aerial Vehicles. he is also a senior research engineer in aeronautics, robotics, and biomedical projects, with the Mohammed VI Polytechnic University. He can be contacted at email: ennaji.moh@gmail.com.



Jaafar Gaber    received the Ph.D. degree in computer science from the University of Science and Technology of Lille, Lille, France, in 1998. He was a Research Scientist at the Institute of Computational Sciences and Informatics, George Mason University, Fairfax, VA. He is currently an associate professor of computational sciences and computer engineering at the University of Technology of Belfort-Montbéliard, UTBW, France. His research interests include high-performance computing, parallel processing, and distributed systems, and experimental performance evaluations. He can be contacted at email: jaafargaber@gmail.com.